ISSN 0016-7029, Geochemistry International, 2006, Vol. 44, No. 5, pp. 501–507. © Pleiades Publishing, Inc., 2006.
Original Russian Text © O.L. Gaskova, 2006, published in Geokhimiya, 2006, No. 5, pp. 548–555.

Influence of Redox Buffers and the Composition of Natural Waters on the Migration of Uranium and Plutonium Accompanying the Disposal of Spent Nuclear Fuel

O. L. Gaskova

Institute of Mineralogy and Petrography, Siberian Division of Russian Academy of Sciences, pr. Akademika Koptyuga 3, Novosibirsk, 630090 Russia

e-mail: gaskova@uiggm.nsc.ru

Received August 15, 2004

Abstract—A thermodynamic model is proposed for the description of U and Pu behavior during their possible leaching from SNF in contact with underground waters. The model is based on the available information on the technology of long-term storage of RAW in geologic environments, the test results obtained in planned and operating disposal sites, and experimental data on the solubility of irradiated U and Pu phases. Water–rock interactions were calculated using the actual compositions of the buffers aimed at suppressing actinide removal from the radiolysis zone and natural ground waters in equilibrium with various rocks. It was supposed that the use of model concentrations in two equilibrium phases for the calculation of distribution coefficients (immobilization if $K_{dis} = M_{solid}/M_{aq}$) provides a fundamental significance to the calculations and may help in the development of predictive models.

DOI: 10.1134/S0016702906050077

INTRODUCTION

Spent nuclear fuel (SNF) contains more than 95% of the total radioactivity of materials involved in human activity [1]. SNF contains 95–98% uraninite, and the remaining part includes various radioisotopes (~1% Pu) produced by nuclear reactions. The construction of underground repositories in deep-seated geologic complexes must involve both natural and artificial (technological) protective barriers decreasing radionuclide migration into the biosphere. Spent fuel in a conserving matrix, a corrosion-resistant container, a buffer from weakly permeable sorption material (bentonites, zeolites, weathered materials), and a water-proof barrier (for example, from concrete) are stored at a maximally possible depth to prevent underground water access to uraninite pellets for hundreds of years [2]. During this time period, short- and medium-lived radioisotopes will decay, and when the geologic environment will be the only barrier, the safety level of the repository will be mainly dependent on the intensity of Pu leakage from SNF and its migration in underground waters. Uraninite is a conserving matrix for this element, which is incorporated in its crystal lattice [1]. Hence, the stability of $UO_{2(s)}$ is a decisive factor.

The aim of this work was to describe covariations of Pu and U contents in underground waters interacting with $UO_{2(s)}$ using a thermodynamic model. At the first stage, the Eh–pH parameters of the reacting solution were maintained by the aforementioned buffers (situation of near-field interaction). Then, particular ground water compositions were taken from the available literature and their interaction with solid phases of actinides or their solutions was evaluated (far-field interaction). Calculation of the equilibrium states for the system considered provides only limited insight into the problem of SNF disposal. Nonetheless, they are important to estimate the possible concentrations of radionuclides in different waters and understand the reason for discrepancies between the observed (based on the results of tests and experiments) and calculated (including conceptual and methodical errors) data.

Program complex and database. The heterophase 14-component system H–O–Cl–K–Na–Ca–Mg–Fe–Al–Si–S–C–U–Pu was modeled at 25°C and 1 bar using the GIBBS algorithm and the UNITHERM database (HCh package) [3]. Data on U and Pu were taken from the NAGRA database [4]. Since these databases are widely accepted and available, we do not present the complete data set of the Gibbs free energies of formation of solid phases and solution species. According to the recommendations of [4], the dissolving dioxides of tetravalent U and Pu were described by thermodynamic potentials ($\Delta_f G^0_{298}$ kJ mol^{-1}) characterizing the stability of their phases with an indefinite degree of crystallinity. Nuclear reactions promote the formation of amorphous phases and also prevent their aging. For this reason, the subscript "s" was used instead of "cr" or "am" for $UO_{2(s)}$ and "hyd,ag" for $PuO_{2(hyd, ag)}$, which denotes a hydrolyzed phase affected by aging. Other reasons for the disagreement between various experimental data on the solubility of actinide dioxides, AnO_2, were previously discussed in [5].

Table 1. Solubility constants ($\log K^0_{sp}$) of oxides and hydroxides of actinides and their Gibbs thermodynamic potentials used in this paper

Phase	Th	U	Pu	ΔfG^0_{298}, kJ mol^{-1}	Reference
$An(OH)_{4(am)}$	–47.0 ± 0.8	–54.5 ± 1.0	–58.5 ± 0.7	–	[6]
$AnO_{2(cr)}$	–54.2 ± 1.3	–60.9 ± 0.4	–64.0 ± 0.5	–	[6]
	–53.2 ± 0.4*	–56.1 ± 1.0**	–58.1 ± 1.0**	–1004.14 $UO_{2(s)}$	[4]
				–963.70 $PuO_{2(hyd, ag)}$	[4]

*Data on the solubility of fine-crystalline Th dioxide.
**Calculated using data from [4] for a reaction corresponding to (1).

Fanghanel and Neck [6] reported the solubility constants of amorphous and crystalline phases of some actinides (Table 1). They expressed the dissolution as

$$MO_n(OH)_{(z-2n)} \cdot xH_2O_{(s)} + (n-x)H_2O = M^{z+} + zOH^-. \quad (1)$$

Then, $K^0_{sp} = [M^{z+}][OH^-]^z(\gamma_M)(\gamma_{OH})^z(a_W)^{(x-n)}$. (2)

Table 1 illustrates the difference in solubility between the crystalline and isostructural amorphous phases. Thorium was included to represent, because there are experimental data on the solubility of its crystalline and fine-grained crystalline phases. The influence of the size of $ThO_{2(s)}$ particles is thus interpolated in [6] by the Schindler equation:

$$\log K^0_{sp}\ (\text{for a particle size of } d) = -54.2\ (\text{crystalline phase}) + 23/d\ (\text{nm}). \quad (3)$$

In particular, $\log K^0_{sp} = -53.2 \pm 0.4$ corresponds to the size of dissolving particles 16–58 nm, and $\log K^0_{sp} = -47.8 \pm 0.3$, 3–8 nm.

Note that the solubility constant of the hydrolyzed dioxide of the highly problematic element Pu most closely matches the solubility of the amorphous phase. Among all the actinides, Pu is most readily hydrolyzed. The hydrolysis of Th^{4+} begins at pH 2.5–3.0; that of U^{4+}, one pH unit lower; whereas Np^{4+} and Pu^{4+} are hydrolyzed already at pH 0–1 [7]. The low rate of $AnO_{2(cr)}$ dissolution and subsequent extensive hydrolysis provide the irreversibility of reaction (4). The $An(OH)_{4(am)}$ phase occurs at the surface and constrain the concentration of actinide in the solution.

$$AnO_{2(cr)} \longrightarrow An_x(OH)^{4x-y}_{y(aq)} \longleftrightarrow An_x(OH)^{4x-y}_{y(col)} \longleftrightarrow An(OH)_{4(am)}. \quad (4)$$

The An content of a solution in equilibrium with colloids before the formation of a solid phase can be estimated by modern physical methods of laser-induced breakdown detection (LIBD) and laser-induced photoacoustic spectroscopy (LPAS), which were used in the experiments of Bitea et al. [8]. At pH 0.8–1.2, there is a reaction producing the second Pu hydroxo complex $Pu(OH)^{2+}_2$, which is in equilibrium with hydroxide or oxyhydrate colloids (5% of total Pu content). The calculated solubility constant of the colloid form is $\log K^0_{sp} = -59.0 \pm 0.3$. Therefore, we believe that the solubility constant of $PuO_{2(hyd, ag)}$ in Table 1 reflects to a first approximation the content of Pu in the solution in truly dissolved and colloidal forms (only intrinsic colloids are considered).

Another important point should be noted. In ultra-acid solutions (where dissolution reactions produce charged ions), the experimental data on An(IV) solubility differ by up to six orders of magnitude according to different authors [4, 6]. The situation changes at pH > 4, when U and Pu concentrations in solution become independent of pH and lie within an interval of two orders of magnitude (without an allowance for $AnO_{2(cr)}$). This observation is used to estimate the accuracy of model calculations constrained by the indicated pH interval.

FACTUAL BASIS AND RESULTS OF MODELING

Tests in planned and operating disposal sites and, especially, experimental data on the solubility of irradiated U and Pu phases indicated that underground waters interacting with SNF show persistent contents of $An \geq 10^{-8}$ mol/l and even up to 10^{-5} mol/l, and radiolysis provides Eh values in the adjacent zone of up to 750 mV [9–14].

In order to simulate actinide precipitation during the interaction with the repository environment (and for the calculation of distribution coefficients), the results of the experiments on SNF solubility (e.g., [15]) can be taken as starting data. These experiments were performed in sealed ampoules filled with Ar or Ar + CO_2 mixture and lasted 545 days. Underground water from granites (pH 7–8) contains 5.4×10^{-5} mol/l U and 1.5×10^{-6} mol/l Pu. Ultrafiltration through a 1.8-nm filter showed that 96% U and 99% Pu occur in a colloidal form.

Materials used as engineering barriers (steel and copper capsules) and potential-controlling redox reactions in natural water–rock systems, primarily, low-temperature (<100°C) reactions between ferric and ferrous Fe [16], must prevent the creation of oxidizing conditions, because their interaction with water is accompanied by intense hydrogen release. Figure 1 shows Eh (V) values for redox pairs, including those for U and Pu. It can be seen that all the pairs (associations) should stabilize $UO_{2(s)}$, $Pu(OH)_{3(cr)}$, and $PuO_{2(hydr, ag)}$, i.e., phases providing a minimum transition of these elements into solution. Among favorable conditions are, first, the closeness of the system and, second, the water–rock regime when electrochemical reactions in the solution are controlled by solid-phase reactions. In such a case, the buffer capacity of geologic environments with artificial barriers can maintain stable conditions and even eliminate the effect of radiolysis, which creates local oxidizing conditions near the surface of SNF. This is confirmed by the efficient preservation of ores in the natural deposit of Oklo, Gabon, and West Africa, which is considered as a natural analogue of SNF repositories [17].

Table 2 shows U and Pu contents in underground waters affected by α-radiolysis and interacting with the aforementioned mineral assemblages. In particular, U(VI) and Pu(VI) minerals can precipitate from highly oxidizing solutions, which were observed in some tests. The material of a steel container (Fe– Fe/Fe_3O_4 buffer) is favorable for actinide immobilization in low-valence compounds, i.e., U(IV) and Pu(III). This fact was recently confirmed by experiments, which, in addition, emphasized the contribution of uranium sorption by magnetite. However, progressive oxidation and the presence of sulfur in water cause a shift toward the FeS_2/Fe_2O_3 buffer (line *7*, Fig. 1), a pH decrease to neutral values, and an increase in Pu(III) content up to 10^{-8} mol/l.

The model bentonite composition corresponds to bentonite MX-80 [19], which is mined in Wyoming and South Dakota and contains about 75% Na-montmorillonite, 15% quartz, 5–8% feldspar, 1.4% carbonates, 0.3% pyrite, and 0.4% C_{org}. The composition of the

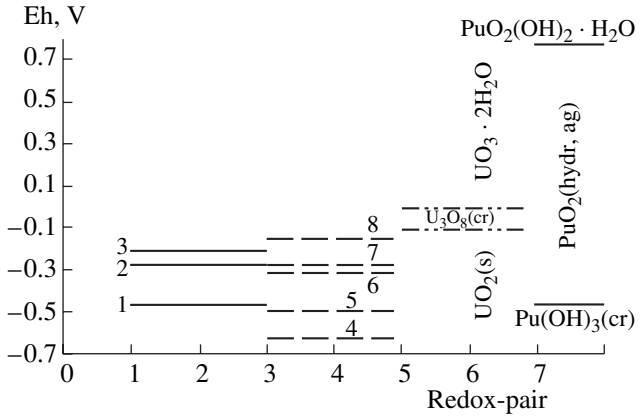

Fig. 1. Redox conditions controlled by various redox pairs: (1) graphite + epidote/calcite + daphnite + quartz + kaolinite, (2) daphnite/pyrite, (3) daphnite/hematite, (4) Fe/Fe_3O_4, (5) Cu/Cu_2O, (6) Fe_3O_4/Fe_2O_3, (7) FeS_2/Fe_2O_3, and (8) $FeCO_3/Fe_2O_3 + C_{org}$. Equilibrium conditions for the main SNF phase, $UO_{2(s)}$, with nonstoichiometric $U_3O_{8(cr)}$ oxide and schoepite $UO_3 \cdot 2H_2O$ formed under oxidizing conditions are shown on the right. Three phases of different Pu valence (III, IV, VI) are given. It is evident that $PuO_{2(hydr, ag)}$ is the most stable at wide variations of Eh values, from those of pore and deep-seated ground waters up to surface waters. Calculations were performed for the interaction of solid phases with water.

pore solution from bentonite was reported in [20]. Calculations showed that its transformation leads to Eh values in the pore water between –0.46 and –0.212 (lines *1–3*). The uranium content of the pore solutions [20] increases up to 4.7×10^{-7} mol/l at the expense of carbonate complexes, because the solution contains up to 52 mmol/l HCO_3^-. However, it was shown [21] that pore solutions in bentonites can have an Na–Cl–SO_4 composition (up to 0.06 mol/l sulfate) with a pH 7.3. In addition, the presence of secondary sulfates and calcite among clay scales indicates a strong Eh shift toward oxidizing conditions. According to [20], a favorable effect can be caused by the addition of Fe(II)-bearing minerals, for example, Fe amphiboles, pyroxenes, chlorites, and fillings and shavings of $Fe_{(el)}$. Calculations

Table 2. Contents of U and Pu in the underground waters of the RAW repositories

Parameter	Radiolysis zone	Fe/Fe_3O_4	Bentonite
Eh, mV	+750	–627	–396
pH	7–8	9.26	8.97
U_{tot}	5.4×10^{-5}	9.86×10^{-10}	4.7×10^{-7}
Main species		$U(OH)_{4(aq)}$	$UO_2(CO_3)_3^{4-}$
Solid phases	$UO_3 \cdot 2H_2O$	$UO_{2(s)}$	$UO_{2(s)}$
Pu_{tot}	1.5×10^{-6}	2.56×10^{-10}	4.3×10^{-11}
Main species		$PuOH^{++}$	$Pu(OH)_4^0$
Solid phases	$PuO_2(OH)_2 \cdot H_2O$	$Pu(OH)_{3(s)}$	$PuO_{2(hydr,ag)}$

Table 3. Composition of the underground waters of various geochemical types (mmol/l), and the U and Pu contents in them (measured and calculated values, mol/l)

Parameter	Ground waters Äspö site [19]	Ground waters Yucca Mountain [22]	Fresh waters of the Siberian platform [23]
pH	7.9	7.4	7.99–6.44
Eh, mV	–280	430	–53
HCO_3^-	1.13	2.1	4.426
Na	51.3	1.99	1.435
K	0.16	0.129	0.141
Ca	18.5 + 0.14 Sr	0.324	0.6
Mg	1.23	0.083	0.395
Fe, tot	5.86×10^{-3}	>0.001	–
Cl	85.4	0.20	0.180
Br	0.199	–	–
I	1.3×10^{-3}	–	–
PO_4^{3-}	3.8×10^{-5}	–	–
SO_4^{2-}	2.76	0.19	–
NH_4^+	0.018	NO_3^- 0.14	0.019
SiO_2	0.068	1.02	–
Al, tot	–	–	–
Li	–	0.009	–
Mn	5.6×10^{-3}	>0.0001	–
An, tot**	U 10^{-9}–10^{-7}	Pu 10^{-10}–10^{-8}	U 10^{-8}–10^{-9}
An, tot	U 10^{-9}	U 2.4×10^{-5}	U 4×10^{-6}
	Pu 10^{-9}	Pu 4.1×10^{-11}	Pu 4.3×10^{-11}
MPC*	^{234}U 5×10^{-6} g/l	^{239}Pu 10^{-9} g/l	
	2.1×10^{-8} mol/l	4.1×10^{-12} mol/l	

*Domestic waters after Laverov et al. [24, p. 8].
**U and Pu contents are taken from the cited publications.

showed that, in such a case, the following reaction causes a decrease in the U content of solutions:

$$UO_2(CO_3)_3^{4-} + 13H_2 = UO_{2(s)} + 3CH_4 + 4OH^- + 5H_2O. \quad (5)$$

Contrasting geochemical types of waters were used to estimate the mobility of actinides in underground waters in the case of the depressurization of engineering barriers and deterioration of their buffer properties (Table 3). These are ground waters from Sweden granites (Äspö site after [19]), Miocene rhyolite tuffs (well J-13 at Jucca Mountain in South Nevada, USA [22]), and fresh waters from the exploited aquifers of liquid RAW repositories in the Siberian platform [23]. The table also shows the maximum permissible concentrations of U and Pu, because the removal of radionuclides by underground waters in dissolved and colloidal forms is directly related to environmental pollution. The data of Table 4 show which solid phases limit the concentrations of dissolved actinides under the given conditions, and which complexes are dominant in the solutions.

It was found that under the reducing conditions of the Äspö site, low-bicarbonate waters have almost identical U and Pb contents (10^{-9} mol/l). However, even this value is 2.5 orders of magnitude higher than MPC of Pu, which is the most dangerous among SNF actinides [25]. This is related to the fact that Pu(III) shows elevated mobility under the reducing conditions of the Äspö site both in acid and neutral waters and can significantly deteriorate the ecological state of water. Hence, geologic conditions providing the formation of acidic solutions are not suitable for SNF disposal.

Yucca Mountain is the only site where long-term disposal of RAW is planned in the aerobic conditions of the undersaturated zone. Under such conditions, U is transformed into highly mobile hexavalent species and can be intensely dissolved:

$$UO_{2(s)} + 1/2O_2 + 2HCO_3^- = UO_2(CO_3)_2^{2-} + H_2O \quad (6)$$

or remain in the solution up to water saturation in uranophane, a complex hydrous Ca–Si uranate. Since Pu occurs under moderately oxidizing conditions in the tetravalent state, the thermodynamic difference between the solubilities of U and Pu oxides can reach almost six orders of magnitude. Hence, negligible (providing preservation of secondary minerals) infiltration in the percolation (aeration) zone is the main requirement for safety.

Fresh bicarbonate waters of underground horizons at Eh ~ 0 (below the stability field of such phases as $UO_3 \cdot 2H_2O$ or β-$UO_2(OH)_2$) are capable of accumulating up to 10^{-6} mol/l of dissolved U owing to the formation of carbonate uranyl complexes. It should be noted that this value is the maximum possible concentration, below which they remain undersaturated and, hence, are potentially aggressive to all U-bearing wastes, ores, and country rocks. Our calculations showed that the high stability of carbonate complexes of UO_2^{2+} significantly reduces the redox potential, which must be maintained at disposal sites to provide stability of the significantly less soluble solid phases of U(IV). An artificial shift toward weaker comlexing anions does not exert a long-term effect, because the waters of exploited horizons are characterized by slow water exchange and return to the geochemical pattern of the host rocks.

Table 4. Minerals, with respect to which ground waters could be oversaturated, solubility-controlling U and Pu solid phases, and main species in the solution

	Äspö site	Yucca Mountain	Siberian platform
Minerals with SI ≥ 1	Fluorite, pyrite, dolomite, apatite, chlorite	Quartz, hematite, dolomite, chlorite	Dolomite
Plutonium	$PuO_{2(hydr, ag)}$	$PuO_{2(hydr, ag)}$	$PuO_{2(hydr, ag)}$
Main dissolved species	Pu^{+++} 2.8×10^{-10}	$Pu(OH)_4^0$ 4×10^{-11}	$Pu(OH)_4^0$ 4×10^{-11}
	$PuOH^{++}$ 4.6×10^{-10}		$PuOH^{++}$ 2×10^{-12}
	$PuSO_4^+$ 1.1×10^{-10}		Pu^{+++} 1.1×10^{-12}
Uranium	$UO_{2(s)}$	Uranophane*	$UO_{2(s)}$
Main dissolved species	$U(OH)_4^0$ 1×10^{-9}	$UO_2(CO_3)_2^{2-}$ 1.3×10^{-5}	$UO_2(CO_3)_2^{2-}$ 2.9×10^{-6}
		$(UO_2)_2(CO_3)(OH)_3^{2-}$ 4.3×10^{-6}	
		$UO_2(CO_3)_3^{4-}$ 2.6×10^{-6}	$UO_2(CO_3)_3^{4-}$ 9.6×10^{-7}

* $Ca[(UO_2)(SiO_3OH)]_2 \cdot 5H_2O_{(s)}$.

DISCUSSION

The results of thermodynamic calculations confirm the main tendencies in the variations of actinide contents in solutions of different compositions occurring under different redox conditions; however, theoretical values are usually lower than experimental ones. The analysis of literature on this problem showed that the discrepancy is due to five main factors: (1) formation of colloids (particles 0.001–1.0 μm in size); (2) intense accumulation of the products of α-radiolysis of water and electrolytes, which is caused by the radioactive decay of radionuclides and shifts local redox equilibria; (3) dissolution of nonstoichiometric and amorphous phases, which usually show both higher solubilities and higher reaction rates; (4) observed stable quasi-equilibrium (steady) state of the apparent oversaturation in chloride solutions owing to factors (1), (2), and (3), in combination with the absence of direct kinetic experimental data on the rate of processes as a function of the most important parameters of the system; and (5) ignoring organic ligands in models, the main of which are acetate, oxalate, and thiocyanate.

As to the problem of migration in a colloidal form, it should be noted that the calculation of saturation indices for ground waters makes it possible to estimate the composition of possible natural microparticles, which will entrap actinides (Table 4). Experimental data [26] indicate that the entrainment of Pu decreases in the sequence hematite ⩾ siliceous colloids > montmorillonite and, in addition, Pu is firmly kept by iron (hydr)oxides, but easily released from silica and montmorillonite. This suggests that those rocks and environments must be used that interact with solutions producing abundant Fe(III) oxides.

Distribution coefficients are usually empirical values related to particular experimental or natural conditions: $K_{dis} = M_{solid}/M_{aq}$, where the numerator is the element content in the solid phase, and the denominator is the element content in the solution. If the calculations involve model contents in two equilibrium phases, such distribution coefficients can be of a more fundamental character. In addition, the analysis of variations caused by changes in the composition of solid phases or solution species can be performed in each point.

Figure 2 shows variations in the distribution coefficients depending on some parameters (Eh, pCO_2, and pH). In particular, uranium is mobile up to Eh 0.11 V, and its content in the solution corresponds to the solubility of schoepite ($UO_3 \cdot 2H_2O$), whereas the solid phase of hexavalent Pu $PuO_2(OH)_2 \cdot H_2O$ was found only under highly oxidizing conditions (Fig. 2a). The redox barrier can be considered efficient only for U, because Pu can be remobilized owing to the appearance of Pu(III) in the solutions. As can be seen in Fig. 2b, K_{dis} of both U and Pu has an opposite trend with decreasing Eh in CO_2-bearing solutions. At Eh = 0.125 V (thin lines), all uranium occurs in the dissolved state even at the lowest $CO_{2(aq)}$ values ($K_{dis} = -1$). Since this zone is characterized by extensive iron oxidation into Fe_2O_3, it can be regarded as promising for uranium precipitation by adsorption on Fe (hydro)oxides, whereas Pu is presumably precipitated as $PuO_{2(hydr, ag)}$. $UO_{2(s)}$ is stable at Eh + 0.0 V (solid lines), but it can be dissolved with the formation of hydroxo- and carbonate complexes of U(VI). Even the carbonate barrier, which is formed, for example, during the consumption of $CO_{2(aq)}$ for the carbonation of cement constructions, permits up to 10^{-6} mol/l U in the solution. It can be seen in Fig. 2c that acidic

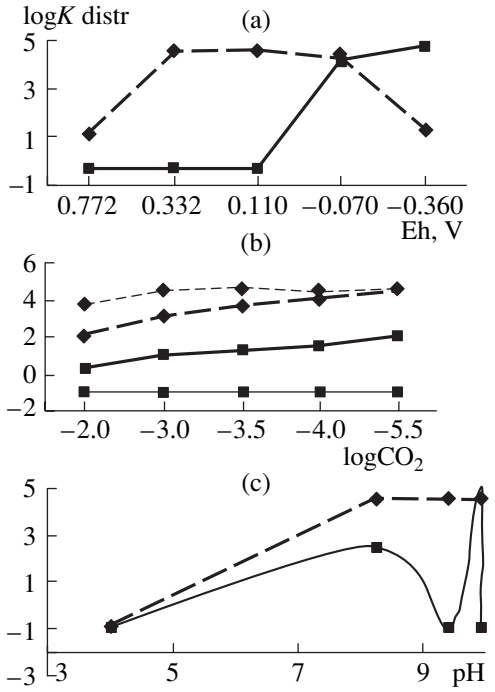

Fig. 2. Distribution coefficients of U (squares) and Pu (diamonds) between solid phases and solution depending on (a) Eh, (b) partial CO_2 pressure, and (c) pH. The value –1 denotes that the actinide occurs only in solution. In panel (b), solid lines correspond to Eh ~ 0.0 V, and thin lines correspond to Eh = 0.125 V and pH 7.4. The pH dependencies (c) were calculated for $pO_2 = –45$ at four values corresponding to the oxidation of $10^{–4}$ mol pyrite, dissolution of calcite, bentonite, portlandite $Ca(OH)_2$, and brucite $Mg(OH)_2$. The latter minerals were taken as the major components of cements used for the isolation of medium-level RAW.

sulfate solutions contain U as UO_2^{2+} (75%) and $USO_{4(aq)}$ (<15%) and Pu as Pu^{3+} and $PuSO_4^+$ in equal amounts. Sharp changes in K_{dis} for U are related to its sensitivity to the presence of Ca ions in the solution (taking into account the $CaUO_4$ phase [27]).

Thus, the quantitative results obtained in this study support the conclusion of very low simultaneous mobility of U and Pu, only in moderately reducing weakly alkaline solutions.

CONCLUSIONS

(1) The use of thermodynamic potentials ($\Delta_f G^0_{298}$ kJ mol$^{–1}$) for amorphized $UO_{2(s)}$ and $PuO_{2(hyd, ag)}$ provides the most adequate description of the solubility of SNF products at a pH > 4.

(2) Even in such a case, the observed experimental contents of actinides are higher than the model values, which can be due to several reasons, including the accumulation of natural colloids. Their compositions can be estimated by calculating the saturation indices of the solution.

(3) The approximate concentrations of U and Pu in the radiolysis zone are close to those in equilibrium with phases of the highest degree of oxidation, $UO_3 \cdot 2H_2O$ and $PuO_2(OH)_2 \cdot H_2O$ according to the NAGRA database.

(4) Three important environmental parameters (Eh, pCO_2, and pH) differently affect U and Pu mobility owing to their distinctive susceptibility to redox reactions, hydrolysis, and formation of secondary compounds and stable complexes in the solutions. This difference can be clearly demonstrated by the calculation of equilibrium interphase distribution coefficients.

ACKNOWLEDGMENT

The work was supported by the Russian Foundation for Basic Research (project nos. 02-05-64623 and 03-05-64548). We are grateful to M.B. Bukaty, N.N. Akinfiev, and D. Kulik (Paul Scherrer Institute, Switzerland) for helpful discussions during the preparation of the manuscript.

REFERENCES

1. N. P. Laverov, V. I. Velichkin, B. I. Omel'yanenko, and S. V. Yudintsev, "Geochemistry of Actinides during the Long-Term Storage and Disposal of Spent Nuclear Fuel," Geol. Rudn. Mestorozhd. **45** (1), 3–23 (2003) [Geol. Ore Dep. **45** (1), 1–21 (2003).
2. *Underground Disposal of Radioactive Wastes* (MAGATE, Vienna, 1981) [in Russian].
3. Yu. V. Shvarov, "Algorithmization of the Numeric Equilibrium Modeling of Dynamic Geochemical Processes," Geokhimiya, No. 6, 646–652 (1999) [Geochem. Int. **37**, 571–577 (1999)].
4. W. Hummel, U. Berner, E. Curti, et al., "NAGRA (National Cooperative for the Disposal of Radioactive Waste)," *PSI Chemical Thermodynamic Data Base, 01/01*, Technical Report 02-16 (2002).
5. O. L. Gas'kova and M. B. Bukaty, "Solubility of Uranium Dioxide during the Underground Disposal of RAW and SNF," Khim. Int. Ust. Razvit. **12** (6), 669–675 (2004) [Chem. for Sustainable Development **12** (6), 649–655 (2004)].
6. Th. Fanghanel and V. Neck, "Aquatic Chemistry and Solubility Phenomena of Actinide Oxides/Hydroxides," Pure Appl. Chem. **74**, 1895–1907 (2002).
7. V. Neck and J. I. Kim, "Solubility and Hydrolysis of Tetravalent Actinides," Radiochim. Acta **89**, 1–16 (2001).
8. C. Bitea, C. Walther, J. I. Yun, et al., "A Study of Colloid Generation and Disproportionation of Pu(IV) in Aquatic Solution by LIBD and LPAS," Proceedings of American Institute of Physics (AIP) Conf. **673** (1), 26 (2003).
9. P. A. Finn, J. S. Hoh, S. F. Wolf, et al., "The Release of U, Pu, Cs, Sr, Tc, and I from Spent Fuel under Unsaturated Conditions," Radiochim. Acta **75**, 65–71 (1996).
10. V. V. Rondinella, H. J. Matzke, J. Cobos, and T. Wiss, "α-Radiolysis and α-Radiation Damage Effects on UO_2

Dissolution under Spent Fuel Storage Conditions," in *Proceedings of 21th Symposium on Scientific Basis for Nuclear Waste Management, Warrendale, 1999*, (MRS, Warrendale) **556**, 447–454 (1999).

11. V. V. Rondinella, J. Cobos, and H. J. Matzke, "Leaching Behavior and α-Decay Damage Accumulation of UO_2 Containing Short-Lived Actinides," in *Proceedings of 24th Symposium on Scientific Basis for Nuclear Waste Management, Pittsburgh, USA, 2001* (MRS, Pittsburgh) **663**, 391–398 (2001).
12. W. Runde, S. D. Conradson, D. W. Efurd, et al., "Solubility and Sorption of Redox-Sensitive Radionuclides (Np, Pu) in J-13 Water from the Yucca Mountain Site: Comparison between Experiment and Theory," Appl. Geochem. **17**, 837–857 (2002).
13. P. V. Amosov, "Simplified Model for the Safety Assessment of the Underground Disposal of High-Level Radioactive Wastes and Spent Nuclear Fuel in Crystalline Rocks (Scenario of Normal Evolution)," Geoekologiya, No. 6, 506–516 (2002).
14. V. Metz, P. Vejmelka, B. Kienzler, et al., "The Effect of a Mg-Oxychlorige–Brucite Backfill Material on the Pu Behavior in $MgCl_2$–NaCl-Brines," Geochim. Cosmochim. Acta. **68** (11S), A511 (2004).
15. A. Loida, B. Grambow, and H. Gecheis, "Congruent and Incongruent Radionuclide Release During Matrix Dissolution of Partly Oxidized High Burnup Spent Fuel," in *Proceedings of 24th Symposium on Scientific Basis for Nuclear Waste Management, Pittsburgh, USA, 2001* (MRS, Pittsburgh) **663**, 417–426 (2001).
16. N. P. Laverov, B. N. Ryzhenko, and Vikt. L. Barsukov, "Some Specific Features of Buffer Redox Reactions in the Rock/Water System," Dokl Akad. Nauk **349**, 381–384 (1996) [Dokl. Akad. Nauk **349A**, 970 (1996)].
17. R. Bros, H. Hidaka, G. Kamei, and T. Ohnuki, "Mobilization and Mechanisms of Retardation in the Oklo Natural Reactor Zone 2 (Gabon)—Inferences from U, REE, Zr, Mo and Se Isotopes," Appl. Geochem. **18**, 1807–1824 (2003).
18. L. Duro, M. Rovira, J. De Pablo, et al., "Sorption and Reduction of Uranium at the Surface of Anoxically Produced Steel Corrosion Products," Geochim. Cosmochim. Acta **68** (11S), A449 (2004).
19. I. Lunden, K. Andersson, and G. Skarnemark, "Modelling of Uranium and Neptunium Chemistry in a Deep Rock Environment," Aquat. Geochem. **2**, 345–358 (1997).
20. N. P. Laverov, B. I. Omel'yanenko, and S. V. Yudintsev, "Isolating Properties of a Bentonite Buffer in Conditions of an Underground Repository for High-Level Radioactive Wastes," Geol. Rudn. Mestorozhd. **46** (1), 27–42 (2004) [Geol. Ore Dep. **46** (1), 22–37 (2004)].
21. D. Kulik, U. Berner, and E. Curti, "Modelling Chemical Equilibrium Partitioning with the GEMS-PSI Code," in *Nuclear Energy and Safety, PSI Scientific Report*, Ed by B. Smith and B. Gschwend (Switzerland, 2004), Vol. 4, pp. 109–122.
22. J. E. Harrar, J. F. Carley, W. F. Isherwood, and E. Raber, *Report of the Committee to Review the Use of J-13 Water in Nevada Nuclear Waste Storage Investigations*, (Lawrence Livermore National Laboratory, Livermore, 1990).
23. M. B. Bukaty, *Migration of Long-Lived Radionuclides in the Deep-seated Storage of RAW GKKh. Research Report* (Tomsk, 2000) [in Russian].
24. N. P. Laverov, B. I. Omel'yanenko, and V. I. Velichkin, "Geological Aspects of the Problem of Radioactive Waste Disposal," Geoekologiya, No. 6, 3–20 (1994).
25. A. P. Korenkov, "On the Classification of Solidified Radioactive Wastes," At. Energ. **73** (2), 129–131 (1992).
26. J. R. Bargar, R. Reitmeyer, J. J. Lenhart, and J. A. Davis, "Characterization of U(VI)-Carbonato Ternary Complexes on Hematite: EXAFS and Electrophoretic Mobility Measurements," Geochim. Cosmochim. Acta **64**, 2737–2749 (2000).
27. I. Grenthe, J. Fuger, R. J. M. Konings, et al., *Chemical Thermodynamics of Uranium* (Elsevier, Amsterdam, 1992), Vol. 1.